PAPER

Dual light-activated microfluidic pumps based on an optopiezoelectric composite

IOP Publishing Journal of Micromechanics and Microengineering
J. Micromech. Microeng. **27** (2017) 125003 (12pp) https://doi.org/10.1088/1361-6439/aa91fc

Dual light-activated microfluidic pumps based on an optopiezoelectric composite

Hsin-Hu Wang[1], Ting-Jui Wu[2], Shih-Jue Lin[3], Jen-Tau Gu[3], Chih-Kung Lee[1,4], I-Chun Cheng[2] and Yu-Hsiang Hsu[1,5]

[1] Institute of Applied Mechanics, National Taiwan University, No. 1, Sec.4, Roosevelt Rd., Taipei 106, Taiwan
[2] Graduate Institute of Photonics and Optoelectronics, National Taiwan University, No. 1, Sec.4, Roosevelt Rd., Taipei 106, Taiwan
[3] Green Rich Technology Co., LTD. No. 31, Keyi St., Chunon, Miaoli 350, Taiwan
[4] Department of Engineering Science & Ocean Engineering, National Taiwan University, No. 1, Sec.4, Roosevelt Rd., Taipei 106, Taiwan

E-mail: yhhsu@iam.ntu.edu.tw

Received 30 March 2017, revised 20 September 2017
Accepted for publication 9 October 2017
Published 30 October 2017

Abstract

In this paper, a new type of microfluidic pump that can be activated and controlled by a masked light source is presented. The actuation of this micropump is based on an optopiezoelectric composite. This composite is constructed by having one of the electrodes of a piezoelectric PVDF (polyvinylidene fluoride) polymer replaced by a layer of TiOPc (titanyl phthalocyanine) photoconductive coating and an ITO (indium-tin-oxide) transparent electrode. This layer of photoconductive electrode provides the capability to activate multiple locations of this optopiezoelectric composite independently using a masked light source and a single voltage source. To verify the feasibility of this concept, dual light-activated microfluidic pumps based on this optopiezoelectric composite are implemented and studied. Experimental results verify that two microfluidic pumps can be created by one optopiezoelectric composite and that each pump can be optically turned on and off independently or be turned on simultaneously. These results suggest that integrating an optopiezoelectric composite into a lab-on-a-chip system can reduce the size and the number of driving units significantly, since every operation can be done optically and only one driving source is needed. The equivalent circuit, design, and implementation of dual light-activated optopiezoelectric micropumps are discussed in this paper.

Keywords: optopiezoelectric composite, optopiezoelectric pump, titanyl phthalocyanine, microfluidic, lab-on-a-chip

S Supplementary material for this article is available online

(Some figures may appear in colour only in the online journal)

1. Introduction

Having the capability to manipulate small liquid samples, microfluidic technology plays an important role in lab-on-a-chip systems. It has become one of the major tools for applications of *in vitro* diagnosis, environmental analysis, biological study, tissue engineering, etc [1, 2]. In order to accomplish complex processing steps on one lab-on-a-chip device and convert devices into commercial products, the operational approaches have been separated into two types of strategies. One type is to use a simple and straightforward mechanism to operate the device. This is often single-use and has a limited number of operations and pausing/incubation steps. Examples include paper-based diagnostic devices [3–5], finger-powered microfluidic devices [6, 7], evacuated-PDMS self-priming devices [8], pump-lid based devices [9], and

[5] Author to whom any correspondence should be addressed.

syringe-based devices [10]. The major applications usually are in the fields of limited-resource-setting (LRS) or patient-self-testing (PST), where a limited power source is available or minimal knowledge of device operation is required.

The second type is devices that usually need an external system to perform complex functions and provide driving power but have the capability to perform much more complex processing steps. The interfacing port usually requires multiple connecting leads, multiple pressurized tubes, or a mechanical apparatus for multiple actuating steps. Examples include electrowetting-on-dielectric (EWOD) based digital microfluidic devices [11, 12], centrifugal force based Lab-on-a-CD devices [13, 14], PDMS pneumatic microvalve based devices [15], and actuator-based systems for activating multiple pumps and valves on a device [11]. Thus, many of the commercial products have a stand-along or portable system with a connecting port for interfacing with microfluidic cartridges. Comprehensive reviews of these designs are found in [16, 17]. Other than these methods, many types of stimulus-active polymer actuators that can integrate with the microfluidic platform also have been reported. These actuators can be activated to create mechanical deformation to serve as valves or pumps by internal or external energy sources, such as electrical, magnetic, optical, or chemical stimulus. A very detailed review of the reported stimulus-active polymer actuators can be found in [18]. In this review, it also is pointed out that the current hurdle for commercializing a lab-on-a-chip device is the necessity of connecting to ancillary hardware for operations. This assembly can be troublesome and not user-friendly.

To overcome this limitation, a user-friendly remote control with minimal connections could be the ultimate solution to bridge lab-on-a-chip technology to commercialization. To achieve this goal, we have conducted a series of studies on developing a new type of piezoelectric composite that can be activated by a light source, named optopiezoelectric composite. This new type of piezoelectric composite uses a layer of photoconductive coating and a transparent electrode to serve as one of the surface electrodes of a piezoelectric thin film. This allows the optopiezoelectric composite to be turned on and off selectively by a masked and programmed light source. It offers the capability to control spatially and temporally the activation of an optopiezoelectric composite, so multiple areas can be controlled dynamically. Embedding this optopiezoelectric composite into a microfluidic system, multiple microfluidic pumps could be created and be optically controlled. This design offers a new operation strategy for a microfluidic platform with a simple and straightforward interface. The number of physical connection interfaces can be reduced to two conducting leads, one being the voltage driving source and the other being the grounding lead. The interface between the external control unit and the device can be simplified significantly, thereby reducing the overall system size. A user-friendly interface can be created and physical connections are simplified considerably.

A similar concept of using a photoconductive material to control a microfluidic device has been applied to light-induced-dielectrophoresis (LIDEP) [19–24] and electrowetting-on-dielectric (EWOD) [24–26] devices. Hydrogenated amorphous silicon (Si:H) [19–22, 25] or titanly phthalocyanine (TiOPc) compounds [23, 24, 26, 27] have been used to replace the electrode of the LIDEP and EWOD devices. This design provides the capability to control dielectrophoresis and electrowetting optically, and microparticles, microdroplets, and cells can be manipulated remotely by a patterned light source. Nevertheless, the magnitude of force and scale is relatively small and the controllable area of optically induced force is limited. Thus, it has been unable to manipulate bulk fluid in a microfluidic system. In this paper, we demonstrates that the optopiezoelectric composite could integrate advantages of both photoconductive and piezoelectric materials. The photoconductive layer provides an interface for optical control, and the piezoelectric actuator provides a mechanical force to manipulate fluid. By using this concept, we could expand the concept of light-induced mechanical control for larger scale applications.

To realize the concept of integrating an optopiezoelectric composite into a microfluidic device for manipulating fluid, a series of TiOPc/PVB composite doped with hole transport materials (HTM) and electron transport materials (ETM) for matching electrical impedance of the piezoelectric polymer (polyvinylidene fluoride; PVDF) was studied. Detailed discussion of this type of photoconductive coating will be presented in a separate paper. In this paper, dual light-activated microfluidic pumps based on this optopiezoelectric composite are implemented to verify the feasibility of using an optopiezoelectric composite to operate two micropumps with a masked light source. The device design, finite element simulation, and experimental study for verifying the feasibility of the optopiezoelectric pump for the application of microfluidics are presented in this paper.

2. Materials and methods

2.1. Design and fabrication of the optopiezoelectric composite

Figure 1(a) shows the configuration of the optopiezoelectric composite designed to integrate into a microfluidic pump. It is composed of a 9 μm thick layer of piezoelectric PVDF thin sheet, purchased from Measurement Specialties, Inc., that has 55 nm Ni/Cu electrodes sputtered on both surfaces. The bottom Ni/Cu electrode first was removed by a $FeCl_3$ (Ferric chloride) solution followed by dip coating a 2 μm thick TiOPc/PVB photoconductive layer. The precursor solution of the TiOPc/PVB coating is composed of α-TiOPc (IT-Chem Co., Ltd) or Y-TiOPc (Sigma-Aldrich Co. LLC.) nanoparticles (NPs) dispersed in a polyvinyl butyral (PVB: Green Rich Technology Co., LTD.; P-90) resin dissolved in cyclohexanone (CYC) and methyl ethyl ketone (MEK) solvent. Butadiene based hole transport material (HTM: Green Rich Technology Co., LTD.; C45) and quinone based electron transport material (ETM: Green Rich Technology Co., LTD.; P44) also were added to the solvent to promote the conductivity of the light-induced electron–hole pair. The weight percentage of the Y-TiOPc NPs was designed to be 50% in the final solid state, and the weight

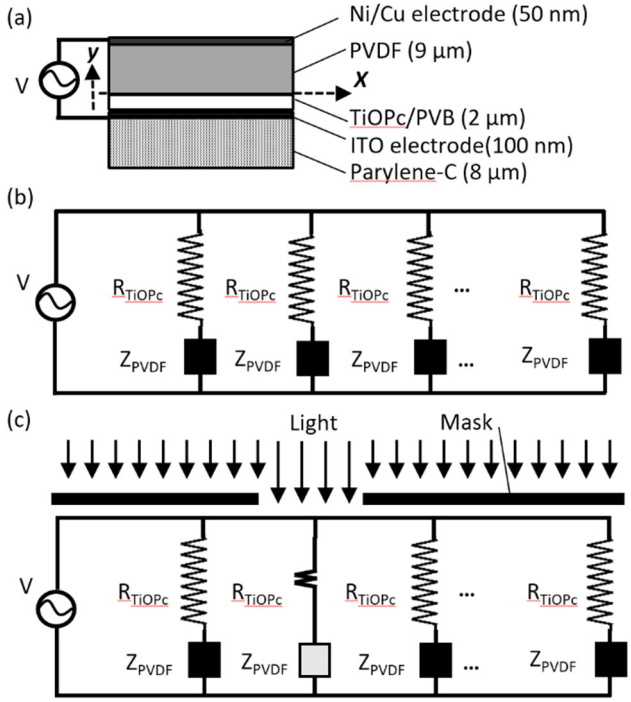

Figure 1. (a) Illustration of the optopiezoelectric composite and equivalent circuits of the optopiezoelectric composite before (b) and after (c) regional activation by a masked light source.

percentage of α-TiOPc was 19%. The ratio of PVB, HTM, and ETM was fixed at 5:4:3 in weight ratio. Then, a layer of 100 nm thick transparent indium-tin-oxide (ITO) electrode was sputter coated on the surface of the TiOPc/PVB surface. This layer of transparent ITO electrode allows a masked light source to activate different regions of the photoconductive layer and serves as the conducting electrode to the electrical driving source.

In order to create a large bending deformation by the piezoelectric effect for creating a large pumping force, a layer of transparent parylene-C polymer was coated on the surface of ITO to move the PVDF thin sheet to one side of the neutral plane of the optopiezoelectric composite, which is the plane remaining undeformed during bending. This is because one side of the neutral plane is subjected to tensile stress and the other is subjected to compressive stress under bending. So, one must control the thickness of each layer to allow the piezoelectric layer located on the same side of the neutral plane to produce the most effective deformation [28]. Since the thicknesses of both Ni/Cu and ITO electrodes are a lot thinner than the PVDF, TiOPc/PVB, and parylene-C layer, their contribution to the flexural rigidity can be neglected. In addition, according to plate theory [29], the resultant force on the cross-section of a pure bending plate must be zero. The optimal thickness of parylene-C controls the neutral plane to be at the interface of the PVDF and TiOPc/PVB. The resultant force can be written as:

$$\sum F_x = \int \sigma \cdot \mathrm{d}A = \int_{y_{NP}}^{y_1} -\left(\frac{E_1 y}{R_1}\right) \mathrm{d}y + \int_{y_{NP}}^{y_2} -\left(\frac{E_2 y}{R_2}\right) \mathrm{d}y + \int_{y_{NP}}^{y_3} -\left(\frac{E_3 y}{R_3}\right) \mathrm{d}y = 0, \quad (1)$$

where E_1, E_2, E_3 are the corresponding elastic modulus of PVDF (2 GPa), TiOPc/PVB (1.9 GPa), and parylene-C (2.8 GPa); h_1, h_2, h_3 are the corresponding thickness of PVDF, TiOPc/PVB, and parylene-C layers; R_1, R_2, R_3 are the corresponding radii of curvature of PVDF, TiOPc/PVB, and parylene-C layers; y_{NP}, y_1, y_2, y_3 are the corresponding y locations of the neutral plane, top surface of the PVDF layer, bottom layers of the TiOPc/PVB, and parylene-C layers. The calculated optimal thickness of parylene-C is 8.02 μm thick. Thus, the thickness of parylene-C deposited on the ITO electrode was chosen to be 8 μm. By designing the optopiezoelectric composite in this unimorph configuration, the piezoelectric thin sheet is placed above the neutral plane and a large bending vibration can be generated by the piezoelectric effect.

2.2. Operation principle of the optopiezoelectric composite

The operating principle of the optopiezoelectric composite can be illustrated by its equivalent circuit. The laminated structure of the optopiezoelectric composite can be represented as many serially connected TiOPc/PVB resistors (R_{TiOPc}) with PVDF impedance (Z_{PVDF}) connected in parallel, as shown in figure 1(b). Using a masked visible light source to activate a portion of the photoconductive layer, the regional resistance of the TiOPc/PVB composite can be reduced three orders of magnitude, as illustrated in figure 1(c). Then, the majority of the driving source (V) applied to this region of the piezoelectric PVDF thin sheet can be estimated by the concept of voltage divider. In this way, the piezoelectric PVDF thin sheet can be actuated to create a large bending vibration and pump fluid. By integrating this mechanism into a microfluidic device, multiple microfluidic pumps can be created with only one driving source.

2.3. Design of the dual light-activated optopiezoelectric pumps

Two microfluidic configurations were designed for developing dual light-activated optopiezoelectric pumps. Figure 2(a) shows the design of dual-pump-A with 50 μm and 200 μm wide serpentine channels connected to the entrance and exit, respectively, of the two micropumps. Figure 2(b) is the second design of dual-pump-B with 50 μm wide serpentine channels connected to both the entrance and exit of both micropumps. The exit of dual-pump-B was connected to one serpentine channel to study the performance of the dual micropumps. The design of dual-pump A is in the opposite direction, where one inlet is separated into two pumps. The observation areas for monitoring the performance of the dual-pumps are highlighted in a dotted gray box. The diameter of each micropump is designed to be 4 mm in diameter, and each connects to microchannels through a valveless nozzle/diffusor to create a directional pumping mechanism (indicated by arrows). The angle of the nozzle/diffusor is designed to be 10°, which is where a maximum flow rate can be achieved, based on reported studies [30, 31]. The serpentine channels are designed for ease of monitoring and quantifying the pumping performance of the dual micropumps.

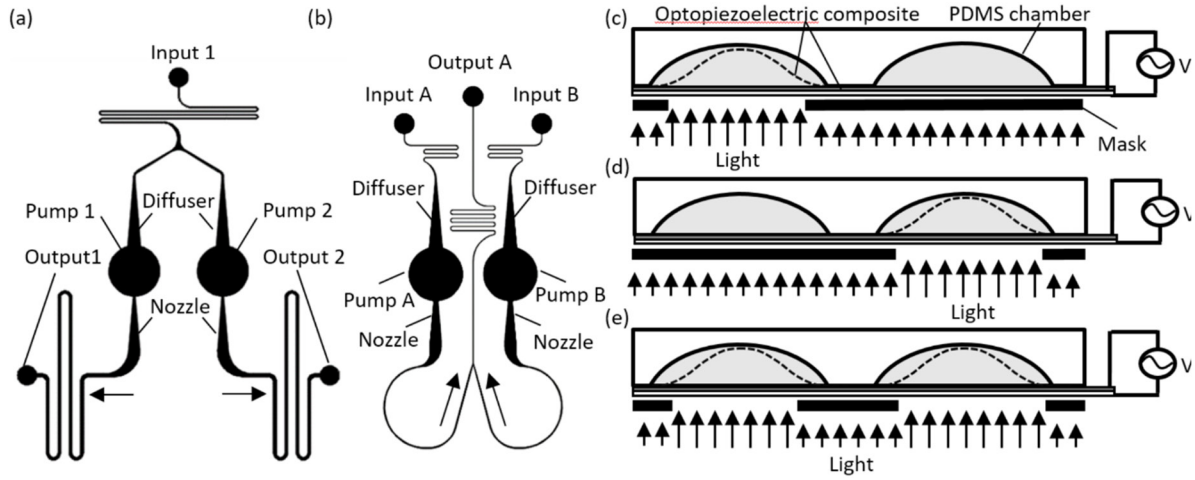

Figure 2. Illustrations of microfluidic configurations of dual light-activated optopiezoelectric pumps, (a) dual-pump-A and (b) dual-pump-B, and its operation principle under the conditions of (c) and (d) one micropump being activated and (e) dual micropumps being activated.

Since the optopiezoelectric composite can provide a large-scale sheet where every location is light excitable, it can be integrated with the PDMS microfluidic channels shown in figures 2(a) and (b). Micromolded PDMS sheets can seal directly with the Ni/Cu surface electrode of the optopiezoelectric composite to create microchannels and let the TiOPc/PVB photoconductive layer face away from the PDMS channel. Then, a masked light source can be placed at the bottom of the optopiezoelectric microfluidic device to control the two micropumps optically. Since the fundamental vibration profile of the optopiezoelectric composite with a circular fixed boundary is similar to a Sinc function (dashed lines, see equation (10)) [29], the PDMS pumping chamber was designed to be a dome shape to increase efficiency. Using this design, the optopiezoelectric pumps selectively can be turned on and off temporally and spatially by illuminating with a visible light source. Thus, one of the dual micropumps can be turned on selectively, as illustrated in figures 2(c) and (d). In addition, they can be turned on simultaneously, as shown in figure 2(e). Most importantly, only one voltage driving source (V) is needed to operate both micropumps.

2.4. Fabrication of the dual light-activated optopiezoelectric pumps

The fabrication procedure of the dual light-activated optopiezoelectric pumps is described briefly in the following. First, three layers of AZ4620 positive photoresist were spin coated sequentially onto a piranha cleaned and HF dipped (1 0 0) silicon wafer. A 46 μm thick AZ4620 coating was created. Then, the standard photolithography process was conducted to expose and develop the designed microfluidic configurations. Then, the developed master was placed on a hotplate at 120 °C for 15 min to allow the photoresist to reflow. The circular pumping chambers were reflowed into a dome-shaped chamber, and the cross-sections of serpentine channels became semi-cylindrical. Standard PDMS micromolding was performed using this master. After curing and demolding the molded PDMS sheet, entrance and exit microchannel holes were punched before sealing the microchannels with the Ni/Cu surface electrode of the optopiezoelectric composite. Two 2 mm thick PMMA sheets were placed on the top and bottom of this assembly to ensure sealing quality by providing a small compressing pressure with eight screws and nuts. 5 mm holes also were cut in the top PMMA sheet to provide fluid access at the entrance and exit of the microfluidic channel (figure 3(a)). Also, 5 mm holes of the locations of the circular micropumps were cut in both PMMA sheets to allow the optopiezoelectric composite to vibrate. Figure 3(b) shows the TiOPc/PVB photoconductive layer (blue film) coated on the piezoelectric layer.

2.5. Analytical analysis of the circular piezoelectric actuator

Based on the theory of the piezoelectric laminate [32], the governing equation of a piezoelectric composite in Cartesian coordinates with 3-axis perpendicular to the surface is

$$D_{11}\left(\frac{\partial^4 w}{\partial x^4}+2\frac{\partial^4 w}{\partial x^2\partial x^2}+\frac{\partial^4 w}{\partial y^4}\right)+\rho h\frac{\partial^2 w}{\partial t^2}= -2G(t)h_{\mathrm{p}}z_{\mathrm{p}}\left[e_{31}\frac{\partial^2 A(x,y)}{\partial x^2}+e_{32}\frac{\partial^2 A(x,y)}{\partial y^2}\right], \quad (2)$$

where w is the bending displacement; D_{11}, ρ, and h are the flexural rigidity, equivalent density, and thickness of the circular piezoelectric actuator; h_{p} and Z_{p} are the thickness and moment arm of the piezoelectric layer with respect to the neutral plane; e_{31} and e_{32} are the piezoelectric stress/charge constants; $G(t)$ are the time domain dependency of the driving voltage source; and $A(x,y)$ is the spatial distribution of the surface electrodes of the piezoelectric actuator.

Since the circular piezoelectric actuator is the basic configuration of the optopiezoelectric pump, the governing equation of the piezoelectric laminate written in polar coordinates is

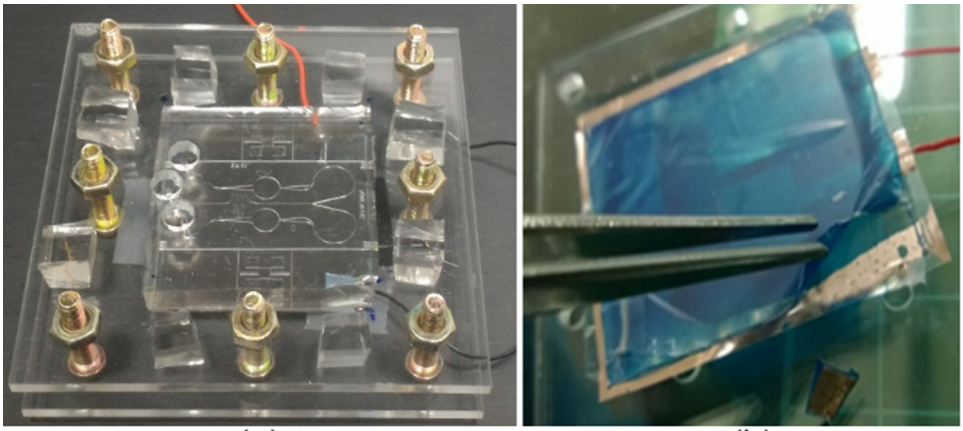

Figure 3. Images of (a) the dual light-activated optopiezoelectric pumps and (b) dip-coated TiOPc/PVB photoconductive layer.

$$\nabla^4 w(r,\theta) - \beta^4 w(r,\theta) = -2G(\omega)h_p z_p \left[e(\theta)\nabla^2 A(r,\theta)\right], \tag{3}$$

where

$$\nabla^4 = \nabla^2\nabla^2 = \left(\frac{\partial^2}{\partial r^2} + \frac{1}{r}\frac{\partial}{\partial r} + \frac{1}{r^2}\frac{\partial^2}{\partial \theta^2}\right)\left(\frac{\partial^2}{\partial r^2} + \frac{1}{r}\frac{\partial}{\partial r} + \frac{1}{r^2}\frac{\partial^2}{\partial \theta^2}\right), \tag{4}$$

and equation (3) has been converted into the frequency domain; ω is the radial frequency; $\beta^4 = \omega^2\rho h/D_{11}$ is the dispersion relationship; $A(r,\theta)$ is the spatial distribution of surface electrode; and $e(\theta)$ is the piezoelectric stress/charge constant, which is a function of θ since e_{31} and e_{32} are not equal in Cartesian coordinates.

Considering the circular piezoelectric composite is clamped on all edges, the boundary conditions are $w(a, \theta) = 0$ and $w'(a, \theta) = 0$. Furthermore, the displacement at center $w(0, \theta)$ is finite. Thus, the general solution is

$$w_{mn}(r,\theta) = [J_m(\beta r) - \frac{J_m(\beta a)}{I_m(\beta a)} I_m(\beta r)] \cos n\theta, \tag{5}$$

where $m = 1,2,3\ldots$ The natural frequencies ω_{mn} are

$$\omega_{mn} = \beta_{mn}\sqrt{\frac{D_{11}}{\rho h}}. \tag{6}$$

Finally, the general solution is

$$w(r,\theta,t) = \sum_{m=0}^{\infty}\sum_{n=0}^{\infty} w_{mn}(r,\theta)T_{mn}(t), \tag{7}$$

Substituting equations (7) into (3) and taking a full field integration with the ij-th w_{ij}(r, θ), the ijth $T_{ij}(t)$ can be found and be written as:

$$T_{ij}(t) = \frac{-2G(t)\int_0^{2\pi}\int_0^a w_{ij}(r,\theta)e(\theta)\nabla^2 A(r,\theta)r\mathrm{d}r\mathrm{d}\theta}{D_{11}(\omega_{ij}^2 - \omega^2)}. \tag{8}$$

Substituting equations (8) into (7), the general solution becomes:

$$w(r,\theta,t) = \sum_{i=0}^{\infty}\sum_{j=0}^{\infty} \frac{-2\int_0^{2\pi}\int_0^a w_{ij}(r,\theta)e(\theta)\nabla^2 A(r,\theta)r\mathrm{d}r\mathrm{d}\theta}{D_{11}(\omega_{ij}^2 - \omega^2)} w_{ij}(r,\theta)G(t). \tag{9}$$

From equation (9), it can be found that the area and location of the surface electrode $A(r, \theta)$ can be designed to maximize the bending deformation of the circular piezoelectric actuator. This is the concept of the effective surface electrode [32], where only the area of piezoelectric laminate having surface electrodes overlapping on both sides can have the piezoelectric effect. This overlapping area is called the effective surface electrode. Furthermore, the location and area of the effective surface electrode can determine the vibration performance and modes of the piezoelectric actuator. In this way, structural vibrations can be enhanced or filtered spatially through the design of the spatial distribution of the surface electrodes. In this study, the photoconductive layer was used to serve as a spatially dynamic electrode, where only the illuminated area can have piezoelectric actuation since only these areas meet the requirements of effective surface electrode.

To achieve a maximum pumping volume, the operation frequency was chosen to be lower or near the first resonance (00th) with zero circular nodal points. Thus, the largest movement of fluid for pumping purposes could be achieved. The vibration mode shape was close to:

$$w_{00}(r,\theta) = \left[J_0\left(10.22\frac{r}{a}\right) - \frac{J_0(10.22)}{I_0(10.22)} I_0\left(10.22\frac{r}{a}\right)\right]. \tag{10}$$

To match this mode shape, a circular effective surface electrode with the center located at the center of the circular piezoelectric actuator was applied. The optimization of the radius of the circular effective surface electrode for creating a large deformation was performed using the finite element method.

2.6. Optimization of the light-activated effective electrode of the optopiezoelectric pump

To identify the optimal radius of the effective surface electrode for a circular optopiezoelectric pump and determine the illuminating area of the photoconductive layer, the MEMS module of the COMSOL multiphysics® software was used to build the numerical model. Since a circular pump in its first circular mode W_{00} is fully symmetric with respect to its center,

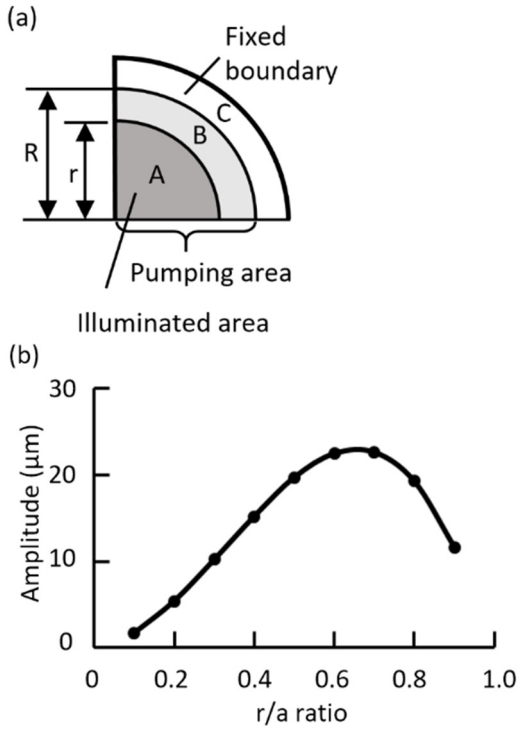

Figure 4. (a) Schematic drawing of the 3D simulation model, and (b) simulated vibration amplitude of the optopiezoelectric circular pump with different surface electrode effect.

only a quarter of the circular pump was simulated and shown in figure 4. The 3D numerical model was separated into three parts, including actuated area (*A*), non-actuated area (*B*), and clamped region (*C*) (figure 4(a)). Since the thickness of PVDF and parylene-C dominates the core of the mechanical structure, only these two layers were built. The optopiezoelectric composite was sandwiched between the micromolded PDMS and PMMA sheets, so the boundary conditions of the top and bottom surfaces of the clamped region (*C*) were set to be fixed and all the other faces on regions (*A*) and (*B*) were set to be free. The total area of the circular pump is defined by regions (*A*) and (*B*) with a fixed radius *a*. The bottom surface of the PVDF layer at both regions (*A*) and (*B*) was grounded for simulating the Ni/Cu electrode. A 160 V driving voltage was applied to the top surface of the PVDF layer at region (*A*) with a varying radius *r* to simulate the effective surface electrode. Piezoelectric material and linear elastic material were set for the top and bottom layers to simulate PVDF and parylene-C layers, respectively. The ratio of radius *r* and *a* was varied from 0.1 to 0.9 with a 0.1 increment. The parameters used in the simulation are as follows. The parylene-C layer is considered an isotropic material, and its Young's modulus and density are $Y_{\text{Parylene-C}} = 2.8\,\text{GPa}$ and $\rho_{\text{Parylene-C}} = 1289\,\text{kg m}^{-3}$. The material parameter of PVDF is based on its mm^2 crystal structure, where the parameters of elastic matrix [*C*] are $C_{11} = C_{22} = C_{33} = 2.27\,\text{GPa}$, $C_{12} = C_{13} = C_{23} = 0.798\,\text{GPa}$, $C_{44} = C_{55} = C_{66} = 0.74\,\text{GPa}$; the piezoelectric stress/charge matrix [*e*] are $e_{31} = 54\ \text{C m}^{-2}$, $e_{32} = 24\ \text{C m}^{-2}$, $e_{33} = -77\ \text{C m}^{-2}$; and the relative permittivity matrix [ε] are $\varepsilon_{11} = \varepsilon_{22} = \varepsilon_{33} = 12.5$ [31]. The damping ratio of the system is 0.1 for both materials. An eigenvalue problem was simulated first to identify the resonant frequency *fr* at the first circular mode. Then, a frequency response of the forced vibration ranging from 0.1*fr* to 4*fr* was conducted to find the vibration amplitude at the central point of the circular pump at resonant frequency under the influence of damping effect.

Figure 4(b) shows the simulated vibration amplitudes of the effective surface electrode with radius *r* varying from 10% to 90% of the total radius *a* of the optopiezoelectric circular pump with 10% increment for each data point (from 0.1 to 0.9). This demonstrates that the driving area defined by the effective surface electrode is closely related to the vibration amplitude. From the simulation results, the optical design of the radius of the effective surface electrode is 0.7*a*, so a 13.29% enhancement of vibrating amplitude can be achieved. Furthermore, a minimal enhancement of 11.32% also can be achieved for the effective surface electrode in the range between 0.5*a* to 0.8*a*. This simulation result suggests that activating the photoconductive layer in this region could provide a larger piezoelectric actuating force to create a larger deformation for pumping fluid.

2.7. Impedance matching circuit of the optopiezoelectric pump

The design of the voltage divider based on the equivalent circuit shown in figure 1 is described here. First, since the pumping system includes the fluidic loading, the optimal driving frequency can decrease significantly [28]. Second, the serpentine channels acted as the interfacing impedance circuit to the overall system. Under these microfluidic configurations, the first measured highest output flow rate of the 4 mm diameter optopiezoelectric pump was at 1 Hz. This suggests that this would be the first resonant mode of this fluidic-structure interaction system. Thus, all of the experimental studies were conducted at this frequency. The equivalent circuit of the PVDF piezoelectric layer can be represented by a capacitor, and the measured capacitance was $C = 1046\ \text{pF cm}^{-2}$. Finally, since the optimal diameter of the effective electrode of a 4 mm circular optopiezoelectric pump is 2.8 mm, the electrical impedance is $|1/j2\pi fC| = 2.471\ \text{G}\Omega$ at $f = 1$ Hz. To use the photoconductive layer to activate the exposed area of the optopiezoelectric composite, the driving voltage applied to the PVDF layer should be low and high during light-OFF and light-ON conditions, respectively. Therefore, the electrical impedance of the PVDF and photoconductive layers must be matched in these two conditions. The driving voltage used in this study was a 180 V_{PP} AC voltage source.

Two types of photoconductive layers were chosen. They provided a compatible Light-ON and Light-OFF resistance to the electrical impedance of the PVDF layer at 1 Hz. The first one was a photoconductive layer consisting of α-TiOPc nanoparticles at 19% solid content doped with HTM and ETM. The thickness of this α-TiOPc/PVB composite was controlled to be 2.0 μm in thickness, and the light-OFF and light-ON resistivity of a 2.8 mm in diameter area was 30.8 GΩ and 0.041 GΩ, respectively. This provides 7.4% (13.32 V_{pp}) and 98.4% (177.12 V_{pp}) percentage of voltage applied to the PVDF layer during light-OFF and light-ON conditions,

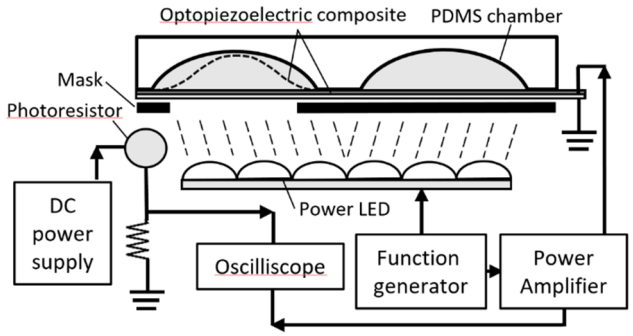

Figure 5. Illustration of the experimental setup for the dual light-activated optopiezoelectric pumps.

respectively. The estimated electric power consumption of the TiOPc photoconductive layer during light-OFF and light-ON conditions were 0.131 μW and 0.027 μW, respectively. The corresponding estimated electric power consumption of the PVDF layer during light-OFF and light-ON conditions were 0.003 μW and 0.515 μW, respectively.

The second type was a 50% Y-TiOPc/PVB photoconductive layer doped with HTM and ETM. The corresponding resistivity of a 2.1 μm thick and 2.8 mm diameter circular region was 24.6 GΩ and 0.0096 GΩ during light-OFF and light-ON conditions. The percentage of voltage applied to the PVDF layer was 9.1% (16.38 V_{pp}) and 90.7% (163.26 V_{pp}) during light-OFF and light-ON conditions. The estimated electric power consumption of the TiOPc photoconductive layer during light-OFF and light-ON conditions were 0.163 μW and 0.006 μW, respectively. The corresponding estimated electric power consumption of the PVDF layer during light-OFF and light-ON conditions were 0.004 μW and 0.438 μW, respectively. The difference between these two photoconductive layers is that the α-TiOPc/PVB composite possesses large unsymmetrical photoconductive characteristics of photo-induced electron–hole pairs. The negative driven portion of the AC voltage can be 12.6 times smaller than the positive part. The 50% Y-TiOPc/PVB composites doped with ETM and HTM have much better symmetricity, where there is a 45% difference between positively and negatively driven voltages. Detailed analysis of the developed TiOPc/PVB composites will be discussed in a separate paper.

3. Experimental

Figure 5 illustrates the experimental setup for verifying the performance of the dual light-activated optopiezoelectric pumps. First, a dual-channel arbitrary function generator (Good Will Instrument Co., Ltd, AFG-2225) was used to generate two synchronized 1 Hz sinusoidal waves with a control phase difference. The first channel was used to apply a constant 180 V AC voltage on the optopiezoelectric composite through a power amplifier (NF Corporation, HSA4052) for driving the dual micropumps. The second channel was to control a power LED for illuminating the two micropumps through different kinds of masks. The driving signal of the optopiezoelectric pump was monitored by sending 1% of the driving voltage to a digital oscilloscope (Tektronix, TDS3054B). The power LED was monitored by a photoresistor through a voltage divider powered by a DC power supply and monitored by the digital oscilloscope. The performance of the dual light-activated optopiezoelectric pumps was monitored and recorded by a stereomicroscope (Olympus, SZX16) and a CCD camera (Olympus, DP80). The recorded video was quantified by ImageJ software. During experiments, dye-colored deionized water first filled the pumping chamber and all three serpentine channels. A portion of the two entrance and exits of three serpentine channels were left unfilled for ease of quantifying the fluidic movement during the operation of the dual light-activated optopiezoelectric pumps. The influence of inertia force can be eliminated.

4. Results

4.1. Selective activation of the dual light-activated optopiezoelectric pumps

To verify that the optopiezoelectric composite can be activated selectively by a masked light source, the dual-pump-A shown in figure 2(a) and 19% α-TiOPC nanoparticles were used. A white light power LED was used to reveal the illuminated area since the major absorbance wavelengths of α-TiOPc are 350 nm and 750 nm. Figures 6(a)–(c) show three experimental results of the dual-pump A being activated by a white light source with different types of masks [33]. Figures 6(a) and (b) are the conditions where only the right (figures 6(a)) or left ((b)) micropump is activated, where a bright spot can be observed in the central regions. Figure 6(c) shows the case where both micropumps can be activated. Due to the majority of the light energy being absorbed and the angle of the picture was taken, the observed light spot looks smaller than 0.7R.

To verify the function of dual-pump A, the white light power LED first illuminated one of the dual pumps for 1 s to activate the photoconductive coating. Then, a 1 Hz 180 V driving voltage was applied immediately to the optopiezoelectric composite. The fluid flow inside the serpentine microchannel at the exit was monitored throughout the process. Following the same procedure, both pumps first were activated by the white light source followed by applying the same driving voltage. Figures 7(a) and (b) show the time-lapse images of the fluid flow over 40 s. Measured volume flow rates and flow rate of these two conditions are shown in figure 7(c), where the circular and rectangular dots represent the dual and single pump, respectively. From the experimental results, a higher volume flow rate results from dual-activated pumps than a single-activated pump. This verifies that the optopiezoelectric pumps selectively can be turned on remotely by a light source. Furthermore, the volume flow rate was highest immediately after activation of the photoconductive layer. The volume flow rate started to decrease over time due to the available photo-induced electron pairs being depleted during the operation. The average volume flow rates at the plateau region were 1.49 nl min^{-1} and 0.33 nl min^{-1} for the dual-activated and single-activated pump, respectively. The corresponding flow rates were 10.83 μm s^{-1} and 2.36 μm s^{-1}. The volume flow rate of

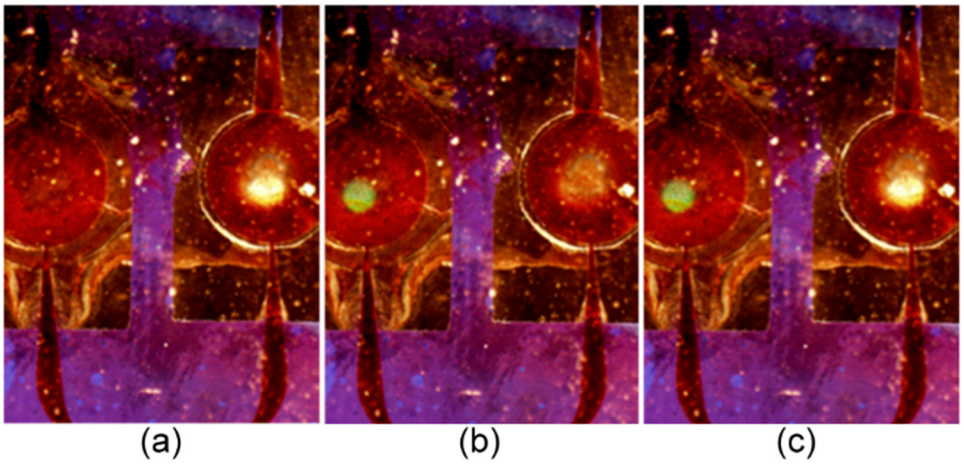

Figure 6. Selective activation of (a) the right micropump, (b) the left micropump, and (c) both micropumps. Reproduced with permission from [33]. [© (2015) COPYRIGHT Society of Photo-Optical Instrumentation Engineers (SPIE). Downloading of the abstract is permitted for personal use only.]

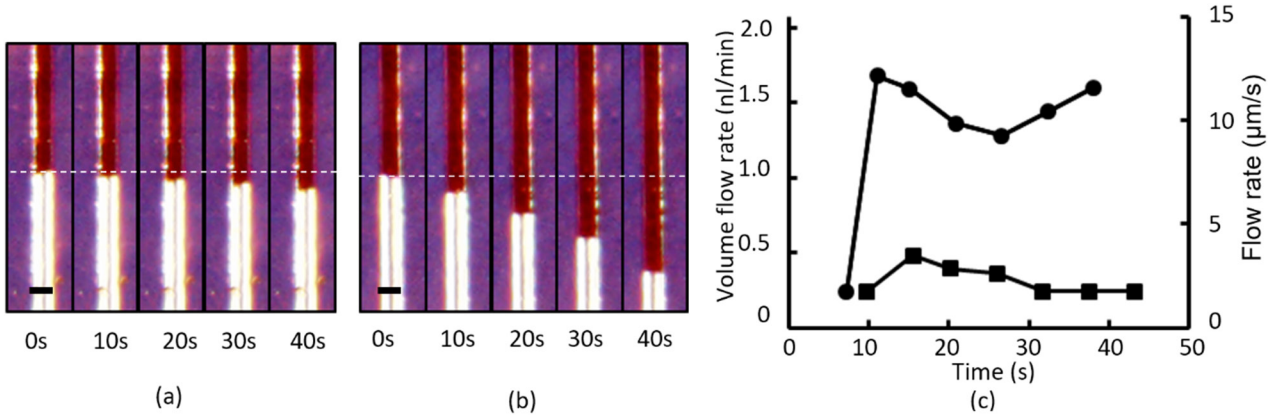

Figure 7. Time-lapse images of fluidic flow driving by activating (a) one micropump and (b) dual pumps, and (c) measured volume flow rate. (scale bar = 50 μm).

the dual-activated pump was 4.6 times greater than a single-activated pump.

4.2. Enhance pumping performance by synchronizing driving voltage and light source

From the experimental finding discussed in the previous section and figure 7, it was found that the pumping performance was highest right after the light was turned off. The flow rate of the dual-activated pump could be above 1.68 nl min^{-1} and 12.2 μm s^{-1}. To enhance pumping performance, the light source was switched on and off synchronously with the driving voltage. This concept was verified using the dual-pump B, where the exit serpentine channel was designed to be between the two micropumps. Thus, the correlation between the dual pumps and the fluidic flow can be monitored simultaneously. Also, to minimize the unsymmetrical behavior of the photoconductive layer, the 50% Y-TiOPc/PVB composites doped with ETM and HTM were used. A red power LED light source with an average of measured energy at 3.37 mW ($\lambda = 635$ nm) was used in this study since TiOPc has the highest absorption spectra in this region. Thus, the majority of the light intensity could be absorbed. Further, both micropumps were turned on and off simultaneously in this case.

The time domain signals of both driving voltage (black line) and measured light intensity (gray line) are shown in figure 8(a). The frequency was fixed at 1 Hz, and the positive portion of the driving voltage was synchronized with the illuminating light source. The illuminating time was only applied for 40% of each cycle, and the piezoelectric pump was activated at the same time. This design could maintain the sinusoidal profile of the driving voltage since the resistivity of the photoconductive layer decreased along with a higher dosage of light. The remaining 60% of the non-illuminated period was used to allow the majority of the remaining photo-induced light source to be discharged. Thus, after each complete cycle, the Y-TiOPc was ready for the next activating cycle. This design was similar to the operating mechanism of a standard Xerographic laser-printing machine.

Figure 8(b) shows the measured volume flow rate using this operating method, where both optopiezoelectric micropumps were activated. The fluidic flow first was stopped in the serpentine channel when the red power LED was turned off. The fluid started to flow once the light was turned on, the measured volume fluidic flow increased to 5.48 nl min^{-1}, and the average volume flow rate was 3.98 nl min^{-1}. The average flow rate was 28.86 μm s^{-1}. Its time-lapse images are shown in figure 8(c). The volume flow rate was 2.67 times

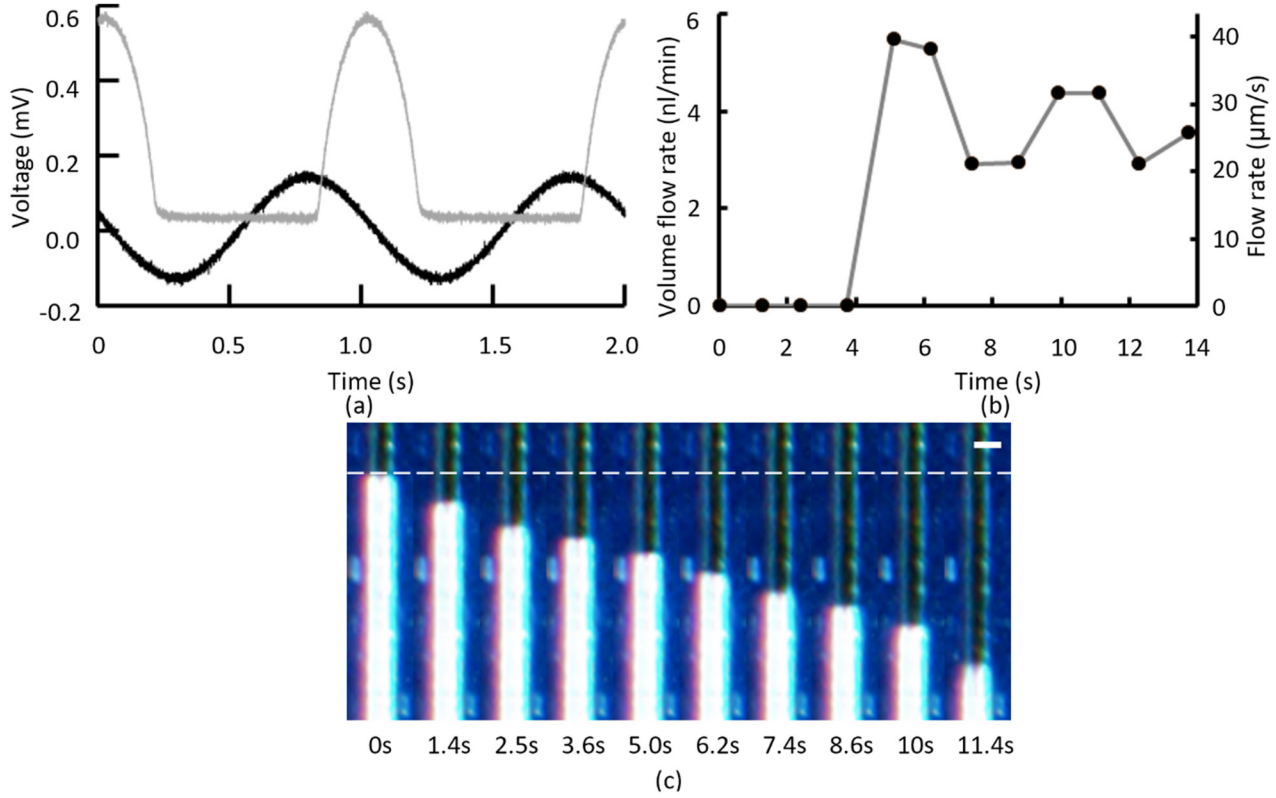

Figure 8. (a) Time domain signals of the driving voltage (black line) and switching light source (gray line), and (b) measured volume flow rate and corresponding (c) time-lapse images of fluidic flow driving by synchronous light and driving voltage (scale bar = 50 μm).

higher than the dual-activated pump shown in figure 7(c). The fluctuation of the measured volume flow rate could be due to the serpentine structure and manufacturing defects of the microchannels. This experimental result demonstrates that the pumping efficiency can be improved significantly using a synchronous light source and driving voltage.

Figure 9 shows the correlation between the leading edge of the fluidic flow (black line) and the activation/deactivation of the optopiezoelectric dual-pump by switching the masked light source ON and OFF (dashed gray line). Both pumps first were activated in the beginning to push fluid flow before being deactivated for 28.5 s followed by activating again. This experiment shows that there was a 6.36 s delay of stopping fluidic flow after the light was turned off. This delay was due to the remaining pressure in the dual-pump needing to be released. Similarly, a 14.36 s delay was found to re-initiate fluidic flow after the light was turned on again. This result showed that a longer time was needed to build pressure against the resistance in the microchannels. This experiment successfully demonstrated that the fluidic flow could be ceased after the illuminating light was turned off and it stopped flowing for 34.5 s. This result verified the optical controllability of the presented optopiezoelectric micropumps. The supplementary video (video-1.avi) shows the recording of this experiment.

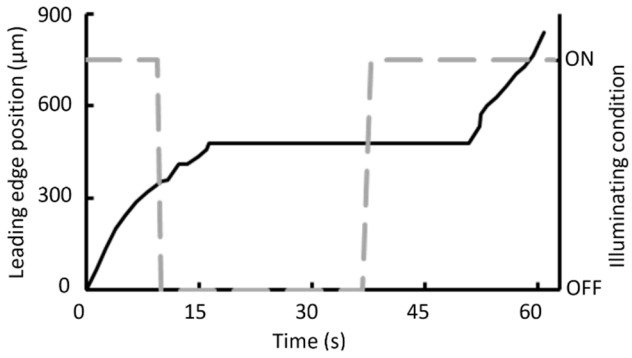

Figure 9. Correlation between fluidic flow (black line; left *y*-axis) and the activation/deactivation of the optopiezoelectric dual-pump by light illumination (dashed gray line; right *y*-axis).

4.3. Contribution of the activating area

To study the contribution of the activating area to the optopiezoelectric pump, we fabricated a simple microfluidic configuration (figure 10(a)) to reduce the hydraulic resistance induced by serpentine channels. Three different circular activating areas were studied, including $r/a = 0.5$, 0.7, and 1.0. Figure 10(b) shows the measured volume flow rates, where the measured average volume flow rates are 0.12 nl min^{-1}, 2.53 nl min^{-1}, and 0.20 nl min^{-1}, respectively. It clearly shows that the volume flow rate can be much enhanced by activating central 70% circular area. This experiment matched simulation result shown in figure 4. It demonstrated that the surface electrode can be used to enhance pumping performance as shown in equation (9). It also suggested that using a larger and smaller activating area, the current design of optopiezoelectric pump could generate sufficient pumping pressure to drive fluidic. However, the resultant volume flow rate was relatively low. It was due to the generated pressure was not sufficient to overcome the drag force induced by the surface

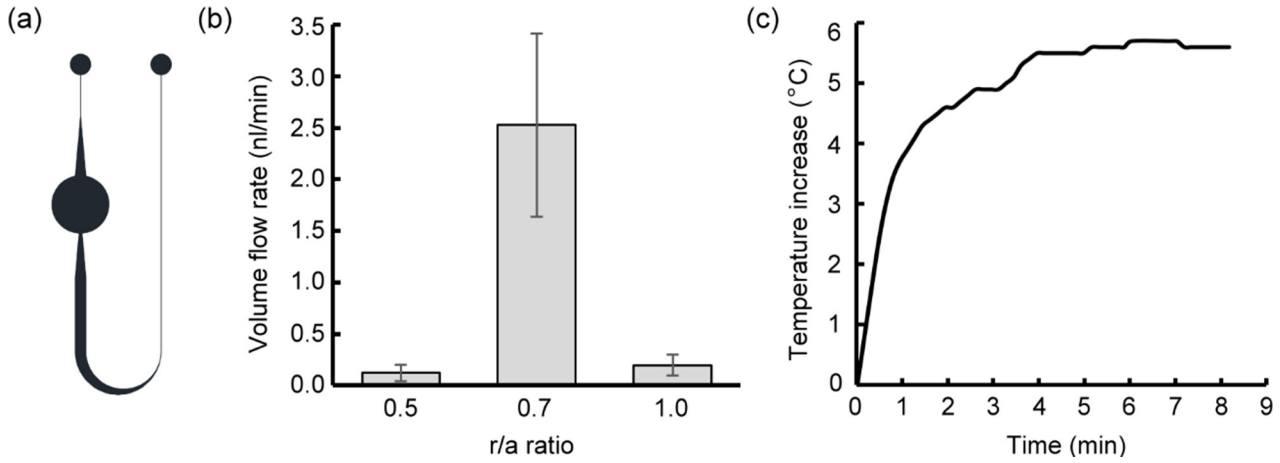

Figure 10. (a) An illustration of the microfluidic configuration of a single optopiezoelectric pump. Experimental results of (b) measured volume flow rates under different activation area and (c) measured temperature increase due to the illuminating light source.

tension at the air–liquid interface. Furthermore, we also found that using the optimal $0.7a$ activating area, the volume flow rate can decreased from an average of 2.53 nl min^{-1} to 1.08 nl min^{-1} under a 1.5 mm H_2O backpressure. Finally, we studied the influence of the light activation to the operating temperature. The measured temperature near the optopiezoelectric pump is shown in figure 10(c). The overall temperature was increased by 5.6 °C in 4 min, and a steady-state condition was reached. This temperature variation did not show a significant influence on pumping performance.

5. Discussions

Our experimental study verified that the optopiezoelectric composite could be integrated with a microfluidic device to create two micropumps. The total number of conducting wires can be reduced from four to two since they can be operated remotely by a masked light source and share one external driving source. Furthermore, it also was verified that these two pumps can be controlled independently or simultaneously using the optical control. The optical control also was studied and showed that, using a synchronized switching light source, the pumping efficiency could be enhanced. These experimental studies clearly demonstrate the concept of the optopiezoelectric micropump.

We would like to emphasize that the integration of the optopiezoelectric composite into a microfluidic device has successfully brought the concept of light-driven droplet/particle manipulation [19] into light-induced bulk fluid manipulation in a microfluidic device. The estimated differential pressure per unit length and pumping force were in the range of sub-Pascal per millimeter and up to several tens of nano-Newtons. It is larger than the pico-Newton force provides by an optical tweezer [34], which is generated by focusing several hundred watts of light energy to a micrometer or a sub-micrometer spot. The operation area of an optical tweezer is small and temperature increase can be significant. It is also larger than the force generated by LIDEP method, which is also in several to over one-hundred pico-Newtown range and the operational area is limited to roughly 10 μm on top of the substrate [20, 24]. On the other hand, the generated pumping force of current configuration is lower than the method of light-induced EWOD [27], which its induced force is assisted by surface tension and can go up to tens of micro-Newtons. However, due to its operation mechanism, its application is limited to droplet manipulations.

Secondly, the optopiezoelectric composite proposed in this paper is not limited to using the 9 μm thick PVDF piezoelectric thin sheet. The choice of this thin PVDF sheet was intended to integrate with the microfluidic device since it is much more flexible than ceramic-type or crystalline piezoelectric materials. Thus, multiple small optopiezoelectric pumps could be designed into a multi-functional microfluidic device to offer multiple optical-controlled micropumps and to achieve multiplex tasks. The pumping performance can further improved by using the derived displacement field of the circular optopiezoelectric actuator shown in equation (9). It suggests that the level of deformation can be enhanced by selecting both the piezoelectric materials and composite composition to adjust the e/D_{11} ratio. For example, the pumping performance of the present design could be improved by using multilayered optopiezoelectric composites, such as a bimorph configuration. The only requirement is to choose a photoconductive layer that has an optical controllable light-ON and light-OFF impedance to match the piezoelectric layer at the operating frequency. The limitation of the driving voltage is the breakdown voltage of the photoconductive layer and the maximum driving voltage of the piezoelectric layer. For the optopiezoelectric composite we developed in this paper, the breakdown voltage of the photoconductive layer was around 30 V μm^{-1}, and the recommended maximum driving voltage of the piezoelectric layer was 30 V μm^{-1}.

Thirdly, an optopiezoelectric composite can be created by replacing one of the surface electrodes of a piezoelectric actuator, such as the ceramic-based piezoelectric micro-pumps summarized in [35]. Similar pumping performance, such as pumping pressure and resistance to back pressure, could be achieved. Thus, all piezoelectric materials can be converted into an optopiezoelectric composite, and all piezoelectric pumps can become optopiezoelectric pumps. Furthermore, its

application is not limited to microfluidic pumps; it can also be applied to all piezoelectric sensors, actuators, valves, motors, and many other applications. Similarly, the method for controlling pumping direction is not limited to the nozzle-diffuser setup.

Finally, since the presented optopiezoelectric pump was developed for manipulating small volume fluid. The pumping performance of current configuration was lower than the majority of reported micropumps. Amirouche *et al* [35] and Iverson *et al* [36] provide detailed reviews on the performance of existing micropumps. The power range of micropumps driven by shape memory alloy, conductive polymer, and piezoelectric actuator are several hundred watts. The micropumps driven by electromagnetic and thermopneumatic methods can go up to several thousands of watts. This power range is much higher than the presented optopiezoelectric pump, which is in the range of sub-micro watts. Furthermore, the level of backpressure of reported methods are in kilopascal range, and it is much higher than the tens Pascal range of presented optopiezoelectric pump. To increase the pumping performace, we can integrate the concept of optopiezoelectric composite into other existing piezoelectric pump, such as a ceramic-based piezoelectric pump and replacing one of the surface electrodes to the photoconductive electrode, a different type of optopiezoelectric composite can be created. Once the impedance of both piezoelectric material and TiOPc layer during light-ON and light-OFF conditions are matched, a similar pumping performance of existing piezoelectric pumps could be reached.

6. Conclusions

In this study, a new type of microfluidic pump based on an optopiezoelectric composite is presented. By integrating the advantages of both photoconductive and piezoelectric materials, multiple locations of the optopiezoelectric composite can be activated selectively by a masked light source both temporally and spatially. The piezoelectric layer at the region of the illuminated area is activated to create a mechanical deformation via the piezoelectric effect. To apply the optopiezoelectric composite in a microfluidic device, both the mechanical structure and electrical impedance are designed. First, the piezoelectric layer is placed on one side of the optopiezoelectric composite to create a large bending deformation. Second, the concept of the effective surface electrode of a piezoelectric laminate is introduced to identify the location and total area of the illuminated region. The finite element method is used to find the optimal condition of the effective surface electrode for the circular pump. This shows that the largest deformation can be created by activating the 70% central area of the circular pump. Third, to control the operation of the optopiezoelectric pump, the equivalent circuit based on a voltage divider is proposed. The electrical impedance of the photoconductive layer and the piezoelectric layer during activated and deactivated conditions must be designed. Using the 19% α-TiOPC/PVB composite, the percentage of voltage applied to the PVDF layer is 7.4% and 98.4% of the total voltage during light-OFF and light-ON conditions, respectively. On the other hand, using a 50% Y-TiOPc/PVB photoconductive layer, the percentage of voltage applied to the PVDF layer is 9.1% and 90.7% during light-OFF and light-ON conditions. This photoconductive layer enables one to control the operation of the piezoelectric layer.

The experimental results demonstrate that the corresponding volume flow rates (flow rate) of a single-activated pump and a dual-activated pump are 0.33 nl min^{-1} (2.36 $\mu m\ s^{-1}$) and 1.49 nl min^{-1} (10.83 $\mu m\ s^{-1}$), when a single light activation for 1 s is used. This verifies the feasibility of using optopiezoelectric composite to control multiple micropumps optically. To improve the pumping efficiency further, the synchronization of the operating frequency of the light source and the driving voltage also is proposed and studied. The average flow rate can be increased to 3.98 nl min^{-1} (28.86 $\mu m\ s^{-1}$). A 267% improvement is achieved. Furthermore, it is verified experimentally that the optopiezoelectric micropumps can be sequentially turned on and off using this clocking light source. Finally, we verified that the pumping performance of a 70% activated pump was 11.1 times larger than a 50% activated pump and 9.1 times larger than a 100% activated pump. This result verified the concept of effective surface electrode and the simulation result.

In summary, the concept of using an optopiezoelectric composite to serve as the core of multiple microfluidic pumps is verified using dual light-activated microfluidic pumps. This demonstrates that, using a single power source and a masked light source, multiple pumps can be controlled optically. This new type of microfluidic pumping method can be integrated into a lab-on-a-chip system. This could reduce the size of the driving unit of a lab-on-a-chip device and the complexity of device design significantly. It also can be scaled up for operating a microfluidic system with complex processing steps.

Acknowledgments

This work is supported by the Ministry of Science and Technology, R.O.C (MOST 106-2628-E-002 -002 -MY3, MOST 105-2221-E-002-160-MY3; MOST 103-2627-E-002-004-). It is also supported by Excellent Research Projects of National Taiwan University (NTU-ERP-105R89081).

Supplementary materials

Video-1.avi: verification the performance of dual light-activated optopiezoelectric pumps (stacks.iop.org/JMM/27/125003/mmedia).

ORCID iDs

Yu-Hsiang Hsu https://orcid.org/0000-0002-9759-7848

References

[1] Haeberle S and Zengerle R 2007 Microfluidic platforms for lab-on-a-chip applications—miniaturisation for chemistry and biology *Lab Chip* **7** 1094

[2] Neethirajan S, Kobayashi I, Nakajima M, Wu D, Nandagopald S and Lin F 2011 Microfluidics for food, agriculture and biosystems industries *Lab Chip* **11** 1574

[3] Martinez A W, Phillips S T, Butte M J and Whitesides G M 2007 Patterned paper as a platform for inexpensive low-volume portable bioassays *Angew. Chem., Int. Ed.* **46** 1318

[4] Rodriguez N M, Wong W S, Liu L, Dewar R and Klapperich C M 2016 A fully integrated paper fluidic molecular diagnostic chip for the extraction, amplification and detection of nucleic acids from clinical samples *Lab Chip* **16** 753

[5] Hu J, Wang S, Wang L F, Pingguan-Murphy B, Lu T J and Xu F 2014 Advances in paper-based point-of-care diagnostics *Biosens. Bioelectron.* **54** 585–97

[6] Iwai K, Shih K C, Lin X, Brubaker T A, Sochol R D and Lin L 2014 Finger-powered microfluidic systems using multilayer soft lithography and injection molding processes *Lab Chip* **14** 3790

[7] Chen A and Pan T 2014 Manually operatable on-chip bistable pneumatic microstructures for microfluidic manipulations *Lab Chip* **14** 3401

[8] Dimov I K, Basabe-Desmonts L, Garcia-Cordero J L, Ross B M, Ricco A J and Lee L P 2011 Stand-alone self-powered integrated microfluidic blood analysis system *Lab Chip* **11** 845

[9] Begolo S, Zhukov D V, Selck D A, Li L and Ismagilov R F 2014 The pumping lid: investigating multi-material 3D printing for equipment-free, programmable generation of positive and negative pressures for microfluidic applications *Lab Chip* **14** 4616

[10] Han K, Yoon Y–J, Shin Y and Park M K 2016 Self-powered switch-controlled nucleic acid extraction system *Lab Chip* **16** 132

[11] McRae M P, Simmons G W, Wong J, Shadfan B, Gopalkrishnan S, Christodoulides N and McDevitt J T 2015 Programmable bio-nano-chip system: a flexible point-of-care platform for bioscience and clinical measurements *Lab Chip* **15** 4020

[12] Malic L, Brassard D, Veres T and Tabrizian M 2010 Integration and detection of biochemical assays in digital microfluidic LOC devices *Lab Chip* **10** 418

[13] Gorkin R, Park J, Siegrist J, Amasia M, Lee B S, Park J–M, Kim J, Kim H, Madou M and Cho Y-K 2010 Centrifugal microfluidics for biomedical applications *Lab Chip* **10** 1758

[14] Strohmeier O, Keller M, Schwemmer F, Zehnle S, Mark D, von Stetten F, Zengerle R and Paust N 2015 Centrifugal microfluidic platforms: advanced unit operations and applications *Chem. Soc. Rev.* **44** 6187

[15] Melin J and Quake S R 2007 Microfluidic large-scale integration: the evolution of design rules for biological automation *Annu. Rev. Biophys. Biomol. Struct.* **36** 213

[16] Boyd-Moss M, Baratchi S, Di Venere M and Khoshmanesh K 2016 Self-contained microfluidic systems: a review *Lab Chip* **16** 3177

[17] Chin C D, Linder V and Sia S K 2012 Commercialization of microfluidic point-of-care diagnostic devices *Lab Chip* **12** 2118

[18] Hilber W 2016 Stimulus-active polymer actuators for next-generation microfluidic devices *Appl. Phys.* A **122** 751

[19] Park S Y and Chiou P Y 2011 Light-driven droplet manipulation technologies for lab-on-a-chip applications *Adv. OptoElectron.* **2011** 909174

[20] Neale S L, Mazilu M, Wilson J I, Dholakia K and Krauss T F 2007 The resolution of optical traps created by light induced dielectrophoresis (LIDEP) *Opt. Express* **15** 12619

[21] Chiou P Y, Ohta A T and Wu M C 2005 Massively parallel manipulation of single cells and microparticles using optical images *Nature* **436** 370

[22] Huang S B, Liu S L, Li J T and Wu M H 2014 Label-free live and dead cell separation method a using high-efficiency optically induced dielectrophoretic (ODEP) force-based microfluidic platform *Int. J. Autom. Smart Technol.* **4** 83

[23] Yang S M, Yu T M, Huang H P, Ku M Y, Hsu L and Liu C H 2010 Dynamic manipulation and patterning of microparticles and cells by using TiOPc-based optoelectronic dielectrophoresis *Opt. Lett.* **35** 1959

[24] Yang S M, Yu T M, Huang H P, Ku M Y, Tseng S Y, Tsai C L, Chen H P, Hsu L and Liu C H 2011 Light-driven manipulation of picobubbles on a titanium oxide phthalocyanine-based optoelectronic chip *Appl. Phys. Lett.* **98** 153512

[25] Shah G J, Ohta A T, Chiou E P, Wu M C and Kim C J 2009 EWOD-driven droplet microfluidic device integrated with optoelectronic tweezers as an automated platform for cellular isolation and analysis *Lab Chip* **9** 1732

[26] Yu T M, Yang S M, Fu C Y, Liu M H, Hsu L, Chang H Y and Liu C H 2013 Integration of organic opto-electrowetting and poly(ethylene) glycol diacrylate (PEGDA) microfluidics for droplets manipulation *Sensors Actuators* B **180** 35

[27] Jiang D and Park S Y 2016 Light-driven 3D droplet manipulation on flexible optoelectrowetting devices fabricated by a simple spin-coating method *Lab Chip* **21** 1831

[28] Ma H K, Chen R H and Hsu Y H 2015 Development of a piezoelectric-driven miniature pump for biomedical applications *Sensors Actuators* A **234** 23

[29] Ventsel E and Krauthammer T 2016 *Thin Plates and Shells: Theory: Analysis, and Applications* (New York: CRC Press)

[30] Jiang X, Zhou Z, Huang X, Li Y, Yang Y and Liu C 1998 Micronozzle/diffuser flow and its application in micro valveless pumps *Sensors Actuators* A **70** 81

[31] Singh S, Kumar N, George D and Sen A K 2015 Analytical modeling, simulations and experimental studies of a PZT actuated planar valveless PDMS micropump *Sensors Actuators* A **225** 81

[32] Lee C K 1990 Theory of laminated piezoelectric plates for the design of distributed sensors/actuators. Part I: governing equations and reciprocal relationships *J. Acoust. Soc. Am.* **87** 1144

[33] Wang H H, Wu T J, Hsu C C, Lee C K and Hsu Y H 2015 A light activated optopiezoelectric thin-film actuator for microfluidic applications *SPIE BiOS* **9320** 93200D

[34] Jun Y, Tripathy S K, Narayanareddy B R J, Mattson-Hoss M K and Gross S P 2014 Calibration of optical tweezers for *in vivo* force measurements: how do different approaches compare? *Biophys. J.* **107** 1474

[35] Amirouche F, Zhou Y and Johnson T 2009 Current micropump technologies and their biomedical applications *Microsyst. Technol.* **15** 647

[36] Iverson B D and Garimella S V 2008 Recent advances in microscale pumping technologies: a review and evaluation *Microfluid. Nanofluid.* **5** 145